ACS OMEGA

Open Access

http://pubs.acs.org/journal/acsodf

Article

Adsorption and Desorption Behaviors of Ammonia on Zeolites at 473 K by the Pressure−Swing Method

Manabu Tokushige and Junichi Ryu*

Cite This: *ACS Omega* 2023, 8, 32536−32543

Read Online

ACCESS | Metrics & More | Article Recommendations | Supporting Information

ABSTRACT: Adsorption and desorption behaviors of ammonia on the zeolites were investigated using the pressure−swing method to utilize the ammonia adsorbent at 473 K. For various (Y, A, L, and mordenite) types of zeolites, the effects of their pore sizes, countercation species, and number of adsorption sites on the ammonia adsorption behavior were evaluated. The adsorption capacity increased with increasing the pore size. The differences in the countercation species and the number of adsorption sites contributed to the ammonia adsorption process on the zeolites. Sodium cations strongly adsorb ammonia molecules. The adsorption/desorption of ammonia expanded and shrunk the zeolite crystal, suggesting that the pores in the zeolite were enlarged by the adsorption of ammonia molecules. Despite repetitive lattice expansion and shrinkage, the morphologies of the zeolite particles were not degraded. These results confirm that the zeolite showed high durability for the adsorption and desorption of ammonia at 473 K.

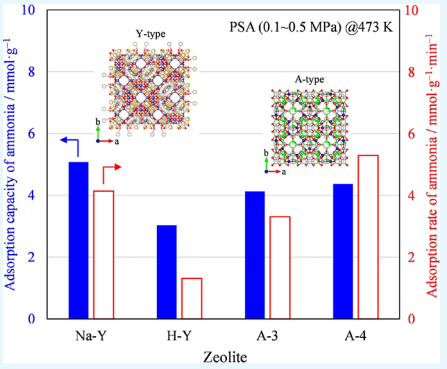

1. INTRODUCTION

Ammonia is one of the most important materials for our planet and prospers our livelihood as a nitrogen-based fertilizer as well as feedstock in various chemical products.[1,2] Additionally, the recent use of renewable energy has made ammonia more attractive as an energy carrier (transportation medium for hydrogen).[2−45] Ammonia has a higher volumetric hydrogen density (121 kg-H_2 m^{-3}) than hydrogen (71 kg-H_2 m^{-3}) and has many advantages as an energy carrier.[1−345] For example, it can be readily decomposed into hydrogen[5] and/or used directly as a fuel.[3,6] Its transportation network is already well established.[3] However, the conventional production process (Haber−Bosch process) requires a huge amount of energy because of the harsh operation under high pressures (20−100 MPa) at a temperature range of 673−873 K, consumes fossil fuels, and exhausts greenhouse gas.[7] Owing to geoenvironmental changes, sustainable ammonia production needs to be innovated.

Meanwhile, the authors and their collaborators developed a small-scale ammonia production method using a ruthenium catalyst.[8−10111213] By using this catalyst, ammonia is synthesized under mild conditions, such as 1.0 MPa at 623 K.[8−10] In addition, small-scale production provides ammonia on demand and on-site. One of the key technologies of this method is the separation and storage of ammonia.[10,14−16171819] Although ammonia is output at 473 K from a reactor,[10,14] it is conventionally cryogenically separated into a liquid state at 240 K.[7] The separation and storage of ammonia at 473 K lowers the heat loss for the cooling and heating circulation of ammonia and reactant gases because ammonia is subsequently and easily collected by a pressure−swing or temperature−swing method. Liu and Aika[15,18,19] confirmed that mixed halide compounds such as $CaCl_2$ and $CaBr_2$ exhibit a high storage capacity for ammonia. Additionally, zeolites show high affinity and stability for ammonia adsorption.[14,17] There are several types of commercially available zeolites based on their crystal types, such as Y-, A-, L-, and mordenite-type zeolites. These zeolites are classified according to their countercation species: proton, sodium, and potassium cation types. The adsorption and desorption behaviors of ammonia on these zeolites at 473 K have not been clarified, although the adsorption/desorption capacities of ammonia and their durability are important for evaluating their feasibility as adsorbents for the separation and storage of ammonia. In this study, we investigated the adsorption/desorption behavior of ammonia on various types of zeolites at 473 K. Seven typical zeolite powders with different crystals and countercation types were examined, and the durability of these zeolites as ammonia storage materials at 473 K was evaluated.

2. MATERIALS AND METHODS

The adsorption/desorption cycles of ammonia on the seven zeolites at 473 K were measured by the pressure−swing method using a magnetic suspension balance (MSB-143,

Received: April 26, 2023
Accepted: August 16, 2023
Published: August 30, 2023

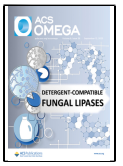

Rubotherm GmbH, Germany). Synthetic Y-type (Na−Y; HS-320 and H−Y; HS-320), A-type (A-3 and A-4), L-type (K−L; HS-500), and mordenite-type (Na−M; HS-642 and H−M; HS-690) zeolite powders were purchased from FUJIFILM Wako Pure Chemical Co. Ltd. Table 1 summarizes the zeolite

Table 1. Zeolite Powders Used in This Study

zeolite	counter cation	pore size (Å)	Si/Al molar ratio	Na_2O (wt %)	particle size (μm)
Na−Y	Na^+	8	3	13	6
H−Y	H^+, Na^+	8	3	4	6
A-3	K^+, Na^+	3	0.5		<75
A-4	Na^+	4	0.5		<75
K−L	K^+, Na^+	8	3	0.2	3
Na−M	Na^+	7	9	5	12
H−M	H^+, Na^+	7	90	0.05	13

powders. The experimental setup is shown in Figure 1. The zeolite powder sample was placed in a platinum basket (ϕ20 × 50 mm) hanging from a magnet, and the basket was suspended by a magnetic force inside a furnace. Before the ammonia adsorption/desorption cycle, the zeolite sample was dehydrated at 493 K under a vacuum for 1 h as pretreatment. After the dehydration, pure ammonia gas (99.9% purity, Resonac Holdings Corp., Japan) was introduced into the furnace at 473 K. The adsorption of ammonia on the sample was conducted at 0.5 MPa ammonia gas pressure for 1 h (pressure−swing adsorption) and the desorption was at 0.1 MPa ammonia gas pressure for 1 h (pressure−swing desorption). The pressure of the ammonia gas was controlled by the temperature of the ammonia tank immersed in an ethanol bath. After the ammonia adsorption/desorption cycles, the sample powders were characterized by using X-ray diffraction (XRD; Ultima IV, Rigaku Corp., Japan), scanning electron microscopy (SEM; JSM-6510A, JEOL Ltd., Japan), and nitrogen adsorption (BELSORP-mini II; Microtrac BEL Corp., Japan). XRD data were obtained for the 2θ range of 5−90° at room temperature with a step interval of 0.01° using Cu-$K\alpha$ radiation, which was determined by calibrating the Si powder. The obtained diffraction patterns were analyzed via the whole powder pattern fitting (WPPF) method[20,21] using PDXL (Rigaku Corp.) with a split pseudo-Voigt function. The corresponding crystal structures were visualized using VESTA.[22] Pore size distribution of the zeolite sample was obtained by the micropore (MP) analysis[23] using BELMaster (Microtrac BEL Corp.) from the nitrogen adsorption isotherm at 77 K.

3. RESULTS AND DISCUSSION

Typical adsorption−desorption cycles of ammonia on the Na−Y zeolite at 473 K are shown in Figure 2. The zeolite showed

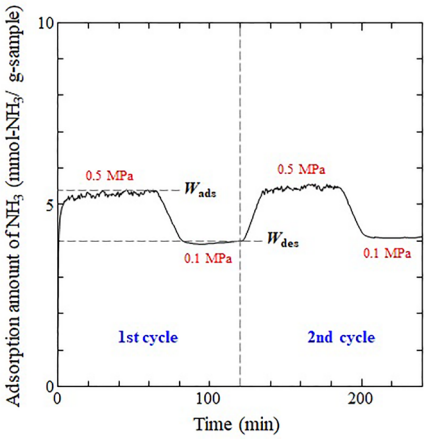

Figure 2. Typical ammonia adsorption/desorption cycles of the Na−Y zeolite at 473 K.

stable adsorption capacity at each pressure of ammonia gas (0.1 and 0.5 MPa), which observed the adsorption/desorption behavior of ammonia on the zeolite at 473 K. The ammonia adsorption capacity in the second cycle was higher than that in the first one. This tendency was observed for all zeolite samples, indicating that the pores were enlarged by the adsorption of ammonia. This phenomenon is discussed at the end of this section, along with the crystallographic refinement results of the zeolites. The results of the ammonia adsorption/desorption cycle examination for each zeolite sample are summarized in Table 2. The adsorption capacity (C_{ads}) and desorption capacity (C_{des}) of ammonia are defined in eqs 1 and 2 as follows:

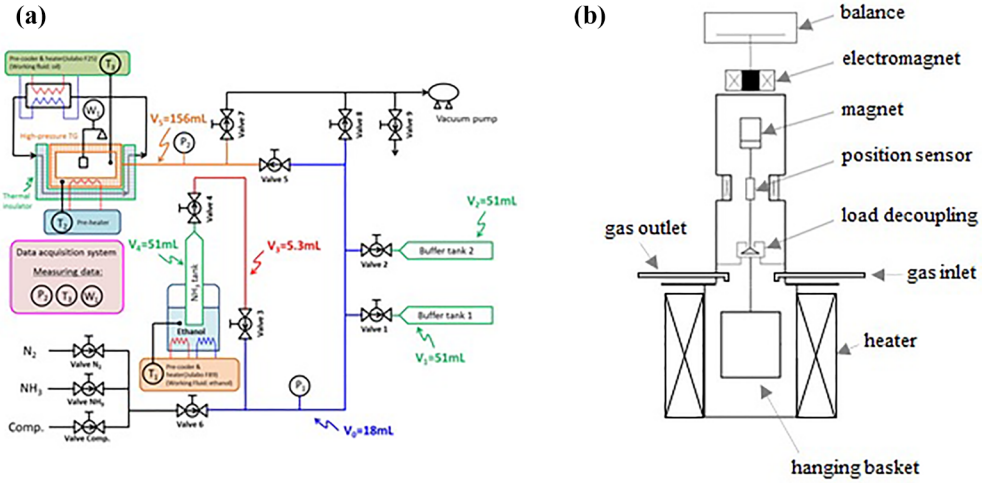

Figure 1. Experimental setup for ammonia adsorption/desorption cycle examination. (a) Gas line and (b) furnace of the magnetic suspension balance.

https://doi.org/10.1021/acsomega.3c02882
ACS Omega 2023, 8, 32536−32543

Table 2. Results of Ammonia Adsorption/Desorption Measurements at 473 K

zeolite	cycle	adsorption capacity, C_{ads} (mmol g^{-1})	adsorption rate, v_{ads} (mmol g^{-1} min^{-1})	desorption capacity, C_{des} (mmol g^{-1})	desorption rate, v_{des} (mmol g^{-1} min^{-1})
Na−Y	first	5.08	4.14	2.18	0.10
	second	5.45	0.59	2.09	0.09
	third	5.63	0.66	2.05	0.10
	fourth	5.63	0.65	2.00	0.08
	fifth	5.44	0.78	1.89	0.09
H−Y	first	3.03	1.31	0.82	0.04
	second	3.10	0.35	0.79	0.04
A-3	first	4.13	3.31	1.45	0.06
	second	4.43	0.49	1.38	0.06
	third	4.49	0.61	1.40	0.06
	fourth	4.52	0.65	1.41	0.06
	fifth	4.58	0.63	1.39	0.06
A-4	first	4.37	5.29	1.31	0.06
	second	4.47	0.82	1.04	0.05
	third	4.67	0.93	1.11	0.05
	fourth	4.69	1.15	1.18	0.05
	fifth	4.60	1.26	1.12	0.05
	sixth	4.60	1.10	1.15	0.05
	seventh	4.55	1.09	1.14	0.05
	eighth	4.52	1.05	1.14	0.05
	ninth	4.54	0.94	1.18	0.05
	10th	4.48	1.07	1.14	0.05

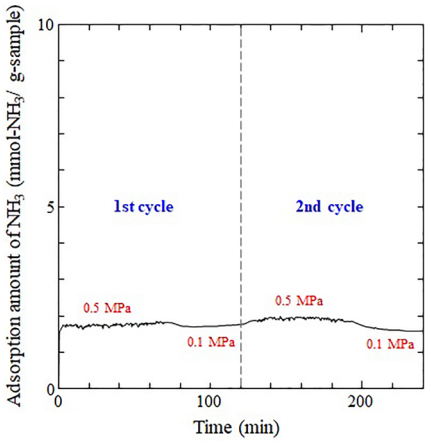

Figure 3. Ammonia adsorption/desorption cycles of the K−L zeolite at 473 K.

$$C_{ads} = \frac{W_{ads} - W_S}{W_S} \quad (1)$$

$$C_{des} = \frac{|W_{des} - W_{ads}|}{W_S} \quad (2)$$

where W_S is the sample weight before the ammonia adsorption/desorption cycle, W_{ads} is the sample weight after the ammonia adsorption cycle, and W_{des} is the sample weight after the ammonia desorption cycle. Furthermore, the adsorption/desorption rates (v_{ads} and v_{des}) were defined as the rates at which 80% of these capacities were achieved in each cycle. The Na−Y zeolite exhibits the highest capacity of ammonia adsorption (5.63 mmol g^{-1}) among the seven types of zeolites. The adsorption capacity of the zeolites increased with increasing pore size. The adsorption capacity of the H−Y zeolite, whose countercation type is a proton, is less than that of the Na−Y zeolite, which agrees with the results of Liu and Aika.[17] They identified the ammonia adsorption sites on the H−Y zeolite using a thermal conductivity detector and Fourier transform infrared spectroscopy. Ammonia adsorbs on the H−Y zeolite via two different processes: Coulombic attraction on alkaline metal cation sites[17] and formation of ammonium ions on proton sites,[17,24] which suggests that the difference in adsorption capacity between Na−Y and H−Y zeolites can be explained by the ratio difference between these adsorption processes, and ammonia adsorption by Coulombic attraction has a larger capacity than the formation of ammonium ions.

The ammonia adsorption capacity of the A-4 zeolite was higher than that of the A-3 zeolite. This was caused not only by their pore sizes but also by their countercation species in the zeolites. The Coulombic attraction from the potassium cation is weaker than that from the sodium cation owing to the lower charge density with a larger ionic radius. A small amount of ammonia was adsorbed onto the potassium cation-type K−L zeolite (Figure 3).

Furthermore, the number of adsorption sites contributed to the adsorption of ammonia on the zeolites. As shown in Figure 4, ammonia slightly adsorbs on the mordenite-type zeolite, for which there are few adsorption sites because of the high Si/Al molar ratio. The number of acid sites in the zeolite is exponentially changed by the Si/Al ratio.[25] Therefore, the number of adsorption sites in the Na−M zeolite drastically differs from that in the Na−Y zeolite. Additionally, the results of XRD measurements confirmed that zeolites were stable against NH_3 adsorption (Figures 5−7, S1, and S2[26−2829]). These results indicate that a larger adsorption capacity for ammonia was obtained with a larger number of adsorption sites in the zeolites.

Regarding the kinetics, the adsorption rate of ammonia on every zeolite was faster than the desorption rate under these experimental conditions. The adsorption rate of ammonia on the A-type zeolite was faster than that on the Y-type zeolite, indicating that the adsorption rate depends on the number of

https://doi.org/10.1021/acsomega.3c02882
ACS Omega 2023, 8, 32536−32543

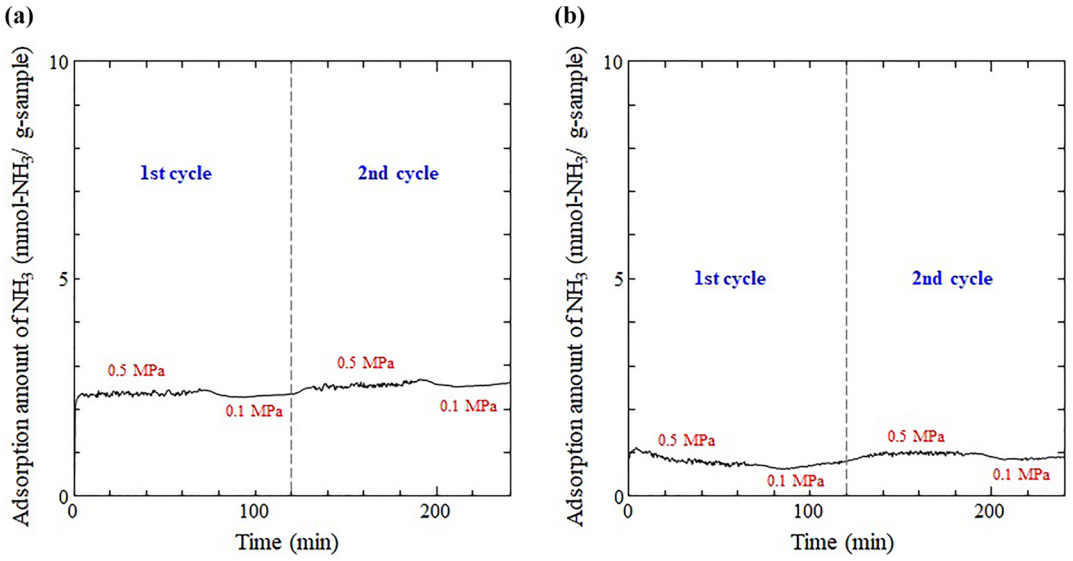

Figure 4. Ammonia adsorption/desorption cycles of mordenite-type zeolites at 473 K. (a) Na−M and (b) H−M.

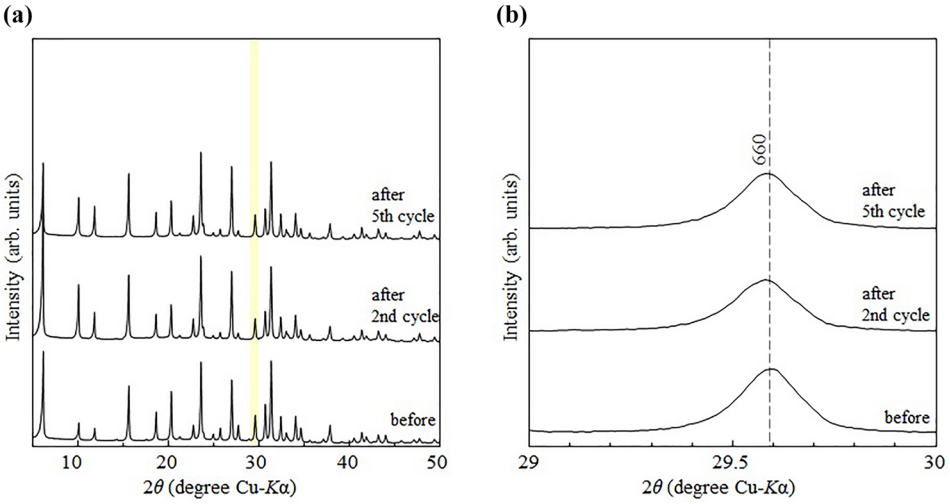

Figure 5. XRD patterns of the Na−Y zeolite before and after ammonia adsorption/desorption cycles at 473 K. (a) 2θ = 5−50° and (b) 2θ = 29−30°.

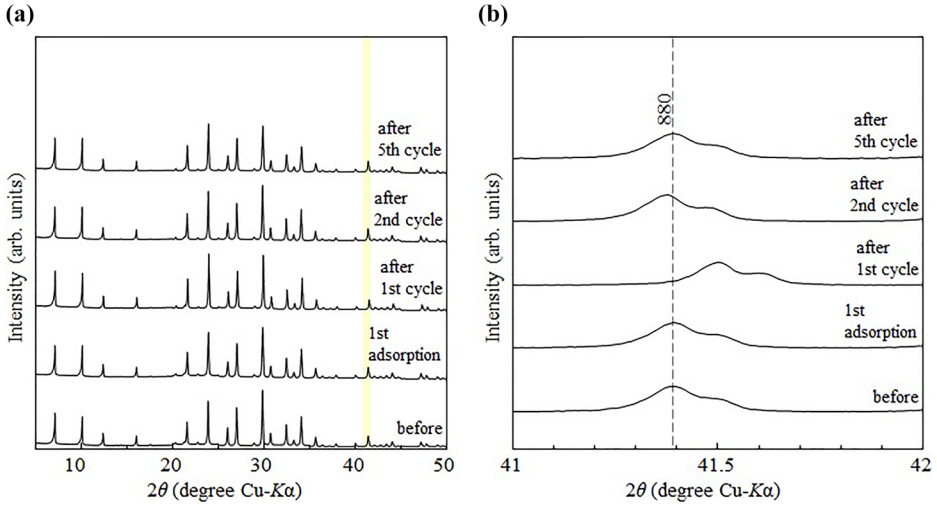

Figure 6. XRD patterns of the A-3 zeolite before and after ammonia adsorption/desorption cycles at 473 K. (a) 2θ = 5−50° and (b) 2θ = 41−42°.

https://doi.org/10.1021/acsomega.3c02882
ACS Omega 2023, 8, 32536−32543

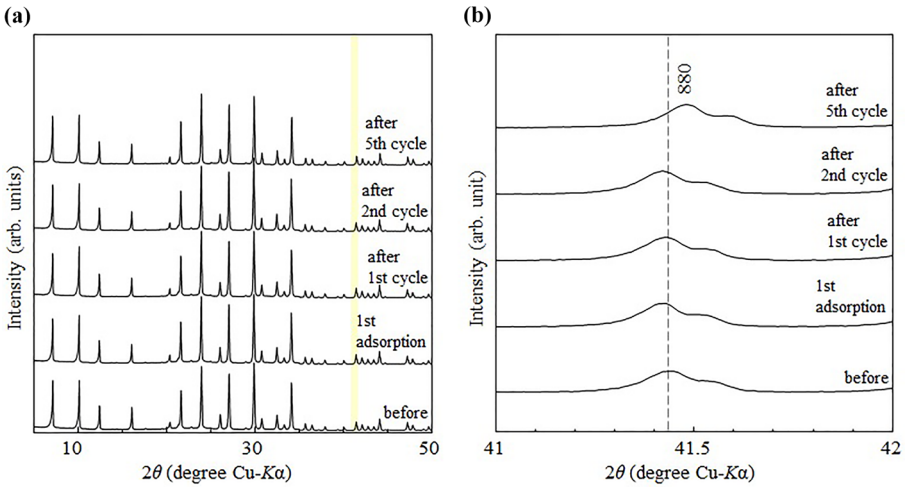

Figure 7. XRD patterns of the A-4 zeolite before and after ammonia adsorption−desorption cycles at 473 K. (a) $2\theta = 5-50°$ and (b) $2\theta = 41-42°$.

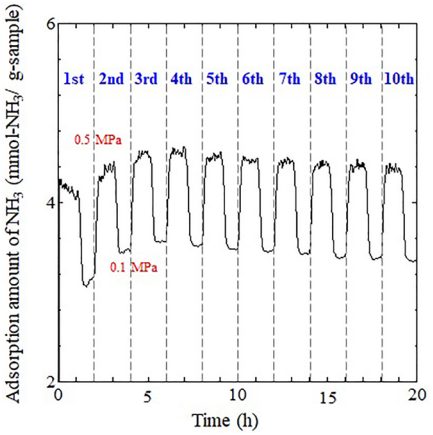

Figure 8. Ammonia adsorption/desorption cycles of the A-4 zeolite at 473 K (10 cycles).

adsorption sites. The contribution of the different counter-cation species to the adsorption process was also observed.

The XRD patterns of the Na−Y zeolite powder after ammonia adsorption/desorption cycles are shown in Figure 5. The observed diffraction patterns were typical of Y-type zeolites with a cubic $Fd\bar{3}m$ structure.[26] The XRD patterns in the 2θ range 29−30° are shown in Figure 5b, indicating the crystal expansion of the Na−Y zeolite after the adsorption/desorption cycle of ammonia. The diffraction peak corresponding to the (660) face shifted to a lower angle by ammonia adsorption/desorption on the Na−Y zeolite. The lattice change is clearly observed in the A-type zeolite, whose pore size is close to the molecular size of ammonia (d_{NH3} = 2.60 Å). The XRD patterns of the A-type zeolites after the ammonia adsorption−desorption cycles are shown in Figures 6 and 7. The observed diffraction patterns were assigned to an A-type zeolite with a cubic $Fm\bar{3}c$ structure.[27] The diffraction peak corresponding to the (880) face was shifted by ammonia adsorption/desorption on the A-type zeolites, indicating the expansion and shrinkage of the A-type zeolite lattice by the adsorption/desorption of ammonia.

To evaluate the durability of the zeolite for ammonia adsorption and desorption, 10 adsorption and desorption cycles were conducted. Figure 8 shows the adsorption/desorption cycles of ammonia on the A-4 zeolite at 473 K.

Table 3. Crystallographic Refinement Results of Zeolites after Ammonia Adsorption/Desorption Cycles

zeolite	crystal	cycle	lattice constant (Å)
Na−Y	cubic	before	a = 24.6430(4)
		second	a = 24.6461(2)
		fifth	a = 24.6421(2)
H−Y		before	a = 24.4958(3)
		second	a = 24.4958(3)
A-3		before	a = 24.6163(2)
		only adsorption	a = 24.6230(2)
		first	a = 24.5703(3)
		second	a = 24.6480(3)
		fifth	a = 24.6235(2)
A-4		before	a = 24.6215(3)
		only adsorption	a = 24.6324(2)
		first	a = 24.6273(3)
		second	a = 24.6240(3)
		fifth	a = 24.5714(2)
		10th	a = 24.6476(3)
K−L	hexagonal	before	a = 18.3687(3), c = 7.5254(1)
		second	a = 18.3699(2), c = 7.5245(1)
Na−M	orthorhombic	before	a = 18.1075(5), b = 20.389(2), c = 7.4988(2)
		second	a = 18.1230(5), b = 20.3888(5), c = 7.5006(2)
H−M		before	a = 18.0844(7), b = 20.2371(6), c = 7.4637(2)
		second	a = 18.0806(7), b = 20.2405(7), c = 7.4618(2)

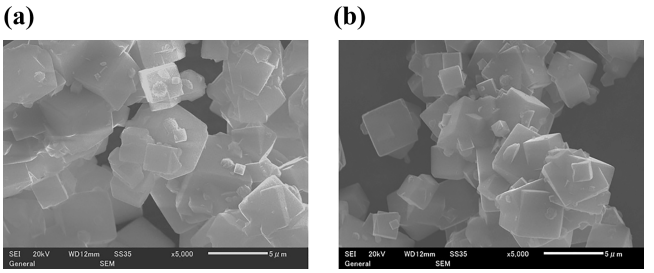

Figure 9. SEM images of the A-4 zeolite before (a) and after the 10th adsorption/desorption cycle of ammonia (b) at 473 K.

https://doi.org/10.1021/acsomega.3c02882
ACS Omega 2023, 8, 32536−32543

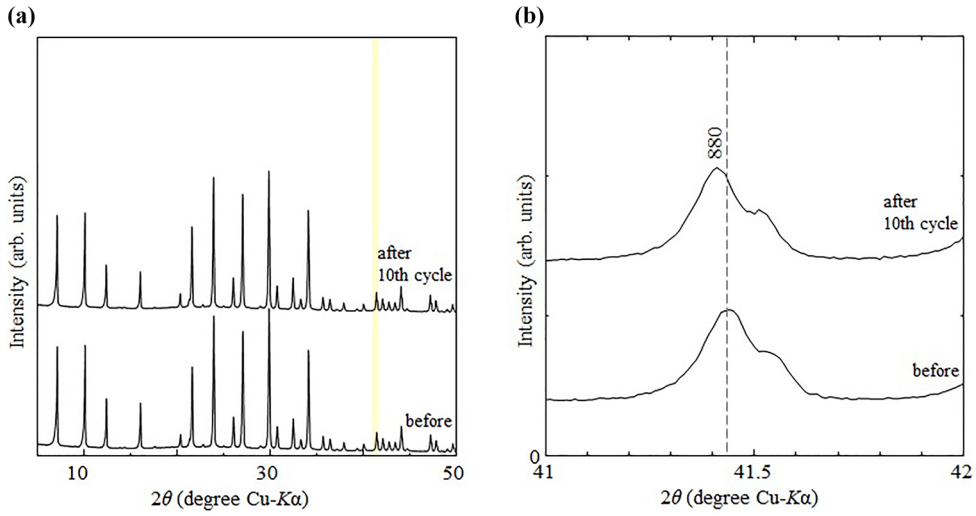

Figure 10. XRD patterns of the A-4 zeolite before and after the 10th adsorption/desorption cycle of ammonia at 473 K. (a) 2 θ = 5−50° and (b) 2 θ = 41−42°.

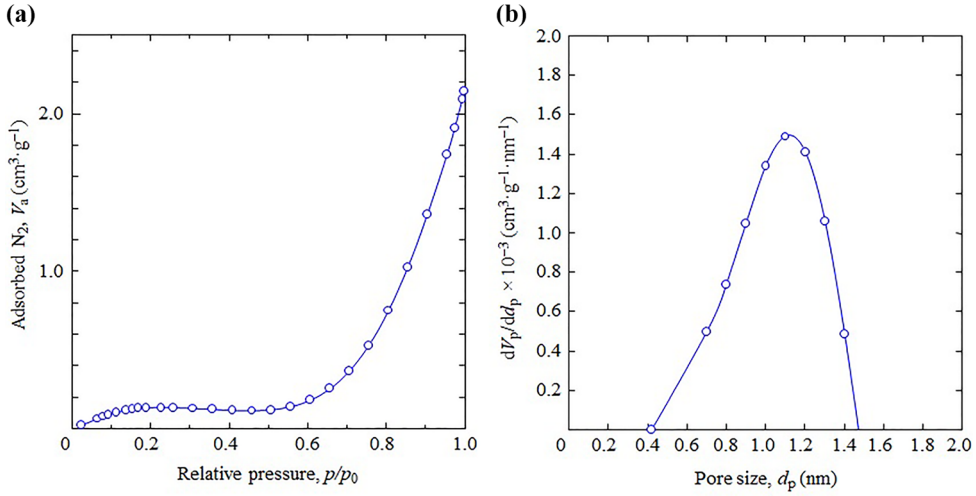

Figure 11. Nitrogen adsorption isotherm (a) and pore size distribution (b) of the A-4 zeolite after the 10th adsorption/desorption cycle of ammonia at 473 K.

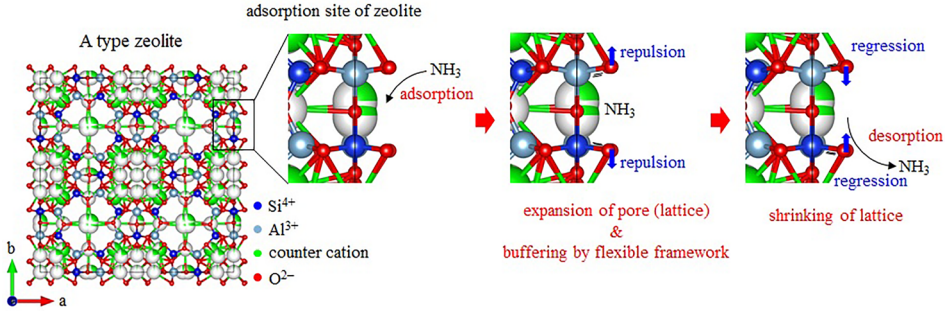

Figure 12. Expansion/shrinkage of the zeolite pore (lattice) by adsorption/desorption of ammonia.

The adsorption capacity of ammonia increased with the number of cycles and subsequently showed a stable value. Therefore, the pores (crystal lattice) of the zeolite were repeatedly expanded or shrunk by ammonia adsorption/desorption cycles. This consideration is supported by crystallographic refinement (Table 3). However, after the 10th cycle, the morphology of the A-4 zeolite particles did not degrade (Figure 9), although the lattice and pore were enlarged (Figures 10 and 11). Although SiO_4 tetrahedra are rigid, corner-sharing between the tetrahedra of SiO_4 and AlO_4 forms an elastic oxide-ion network (flexible window) in the zeolite.[30,31] Considering that the corner-sharing structure induces flexibility in the zeolite, the Si/Al molar ratio defines the flexibility. As shown in Figure 12, when an ammonia molecule adsorbs on the countercation (adsorption site) inside the zeolite pore, the pore (lattice) is enlarged with the oxide

https://doi.org/10.1021/acsomega.3c02882
ACS Omega 2023, 8, 32536−32543

ion repulsed by the Coulombic force from the trivalent nitrogen anion and shrinks owing to the desorption of ammonia. However, this expansion/shrinkage of the pores (lattice) was buffered by the flexibility of the zeolite framework, and the morphology of the zeolite particles was not degraded. These results confirm that the zeolite was stable toward the adsorption/desorption of ammonia at 473 K.

4. CONCLUSIONS

The adsorption and desorption behaviors of ammonia on the zeolites at 473 K were investigated by using the pressure−swing method. The effects of pore size, countercation species, and the number of adsorption sites on ammonia adsorption behavior were evaluated for various types of zeolites (Y-, A-, L-, and mordenite-type). Among them, the Na−Y zeolite exhibits the highest adsorption capacity of ammonia (5.63 mmol g^{-1}). The ammonia adsorption capacity increased with larger pore sizes in the zeolites. The A-4 zeolite exhibits the highest adsorption rate of ammonia (5.29 mmol g^{-1} min^{-1}). The adsorption rate of ammonia on the zeolite was faster than its desorption rate. The adsorption rate depended on the number of adsorption sites. Sodium cations strongly adsorb ammonia molecules. The adsorption/desorption of ammonia resulted in the expansion/shrinkage of the zeolite crystals, which suggests that the pores in the zeolites were enlarged by ammonia adsorption. However, expansion of the zeolite lattice was buffered by its flexibility, and the zeolite particles were not degraded. The adsorption and desorption behaviors of ammonia on the zeolites were observed, and their stability toward these processes was confirmed at 473 K.

■ ASSOCIATED CONTENT

Supporting Information

The Supporting Information is available free of charge at https://pubs.acs.org/doi/10.1021/acsomega.3c02882.

XRD patterns of K−L zeolites before and after second ammonia adsorption/desorption cycle at 473 K at 2 θ = 5−50° and 2 θ = 24−26° (Figure S1), XRD patterns of mordenite-type zeolites before and after second ammonia adsorption/desorption cycle at 473 K at 2 θ = 5−50° and 2 θ = 25−27° (Figure S2), nitrogen adsorption isotherm and pore size distribution of the A-3 zeolite after second adsorption/desorption cycle of ammonia at 473 K (Figure S3), and reliability factors of crystallographic refinements (Table S1) (PDF)

■ AUTHOR INFORMATION

Corresponding Author

Junichi Ryu − *Graduate School of Engineering, Chiba University, Chiba 263-8522, Japan;* orcid.org/0000-0003-2248-8644; Phone: +81-43-290-3128; Email: jryu@chiba-u.jp

Author

Manabu Tokushige − *Graduate School of Engineering, Chiba University, Chiba 263-8522, Japan*

Complete contact information is available at: https://pubs.acs.org/10.1021/acsomega.3c02882

Notes

The authors declare no competing financial interest.

■ ACKNOWLEDGMENTS

This research was supported by Science and Technology Research Partnership for Sustainable Development (SATREPS) in collaboration between Japan Science and Technology Agency (JST, JPMJSA2104) and Japan International Cooperation Agency (JICA). We also thank Mr. Shun Mashiko and Mr. Morihiro Suzuki for their preliminary experiments.

■ REFERENCES

(1) Erisman, J. W.; Sutton, M. A.; Galloway, J.; Klimont, Z.; Winiwarter, W. How a century of ammonia synthesis changed the world. *Nat. Geosci.* **2008**, *1*, 636−639.

(2) MacFarlane, D. R.; Cherepanov, P. V.; Choi, J.; Suryanto, B. H. R.; Hodgetts, R. Y.; Bakker, J. M.; Ferrero Vallana, F. M. F.; Simonov, A. N. A roadmap to the ammonia economy. *Joule* **2020**, *4*, 1186−1205.

(3) Valera-Medina, A.; Xiao, H.; Owen-Jones, M.; David, W. I. F.; Bowen, P.-J. Ammonia for power. *Prog. Energy Combust. Sci.* **2018**, *69*, 63−102.

(4) Lan, R.; Irvine, J. S. T.; Tao, S. Synthesis of ammonia directly from wet air at intermediate temperature. *Int. J. Hydrog. Energy* **2012**, *37*, 1482−1494.

(5) Lamb, K. E.; Dolan, M. D.; Kennedy, D. F. Ammonia for hydrogen storage; A review of catalytic ammonia decomposition and hydrogen separation and purification. *Int. J. Hydrog. Energy* **2019**, *44*, 3580−3593.

(6) Zhao, Y.; Setzler, B.-P.; Wang, J.; Nash, J.; Wang, T.; Xu, B.; Yan, Y. An efficient direct ammonia fuel cell for affordable carbon-neutral transportation. *Joule* **2019**, *3*, 2472−2484.

(7) Liu, H. Ammonia synthesis catalyst 100 years: practice, enlightenment and challenge. *Chin. J. Catal.* **2014**, *35*, 1619−1640.

(8) Aika, K.; Hori, H.; Ozaki, A. Activation of nitrogen by alkali metal promoted transition metal I. Ammonia synthesis over ruthenium promoted by alkali metal. *J. Catal.* **1972**, *27*, 424−431.

(9) Aika, K. Heterogeneous catalysis of ammonia synthesis at room temperature and atmospheric pressure. *Angew. Chem., Int. Ed.* **1986**, *25*, 558−559.

(10) Aika, K.; Kakegawa, T. On-site ammonia synthesis in De-NOx process. *Catal. Today* **1991**, *10*, 73−80.

(11) Ogura, Y.; Asai, T.; Sato, K.; Miyahara, S.; Toriyama, T.; Yamamoto, T.; Matsumura, S.; Nagaoka, K. Effect of calcination and reduction temperatures on the catalytic activity of $Ru/La_{0.5}Ce_{0.5}O_{1.75}$ for ammonia synthesis under mild conditions. *Energy Technol.* **2020**, *8*, No. 2000264.

(12) Sato, K.; Nagaoka, K. Boosting ammonia synthesis under mild reaction conditions by precise control of the basic oxide−Ru interface. *Chem. Lett.* **2021**, *50*, 687−696.

(13) Miyahara, S.; Sato, K.; Kawano, Y.; Imamura, K.; Ogura, Y.; Tsujimaru, K.; Nagaoka, K. Ammonia synthesis over lanthanoid oxide−supported ruthenium catalysts. *Catal. Today* **2021**, *376*, 36−40.

(14) Liu, C.-Y.; Aika, K. Modification of active carbon and zeolite as ammonia separation materials for a new de-NOx process with ammonia on-site synthesis. *Res. Chem. Intermed.* **2002**, *28*, 409−417.

(15) Liu, C.-Y.; Aika, K. Absorption and desorption behavior of ammonia with alkali earth halide and mixed halide. *Chem. Lett.* **2002**, *31*, 798−799.

(16) Liu, C.-Y.; Aika, K. Effect of surface oxidation of active carbon on ammonia adsorption. *Bull. Chem. Soc. Jpn.* **2003**, *76*, 1463−1468.

(17) Liu, C.-Y.; Aika, K. Ammonia adsorption on ion exchanged Y-zeolites as ammonia storage material. *J. Jpn. Petrol. Inst.* **2003**, *46*, 301−307.

(18) Liu, C.-Y.; Aika, K. Ammonia absorption on alkaline earth halides as ammonia separation and storage procedure. *Bull. Chem. Soc. Jpn.* **2004**, *77*, 123−131.

(19) Liu, C.-Y.; Aika, K. Ammonia absorption into alkaline earth metal halide mixtures as an ammonia storage material. *Ind. Eng. Chem. Res.* **2004**, *43*, 7484−7491.
(20) Pawley, G. S. Unit-cell refinement from powder diffraction scans. *J. Appl. Crystallogr.* **1981**, *14*, 357−361.
(21) Toraya, H. Whole-powder-pattern fitting without reference to a structural model: application to X-ray powder diffraction data. *J. Appl. Crystallogr.* **1986**, *19*, 440−447.
(22) Momma, K.; Izumi, F. VESTA 3 for three-dimensional visualization of crystal, volumetric and Morphology Data. *J. Appl. Crystallogr.* **2011**, *44*, 1272−1276.
(23) Mikhail, R.Sh; Brunauer, S.; Bodor, E. E. Investigations of a complete pore structure analysis: I. Analysis of micropores. *J. Colloid Interface Sci.* **1968**, *26*, 45−53.
(24) Earl, W.-L.; Fritz, P.-O.; Gibson, A. A. V.; Lunsford, J.-H. A solid-state NMR study of acid sites in zeolite Y using ammonia and trimethylamine as probe molecules. *J. Phys. Chem.* **1987**, *91*, 2091−2095.
(25) Celik, F. E.; Kim, T. J.; Bell, A. T. Effect of zeolite framework type and Si/Al ratio on dimethoxymethane carbonylation. *J. Catal.* **2010**, *270*, 185−195.
(26) Seo, S. M.; Kim, G. H.; Lee, H. S.; Ko, S. O.; Lee, O. S.; Kim, Y. H.; Kim, S. H.; Heo, N. H.; Lim, W. T. Single-crystal Structure of Fully Dehydrated Sodium Zeolite Y (FAU), $\|Na_{71}\|[Si_{121}Al_{71}O_{384}]$-FAU. *Anal. Sci. X-ray Struct. Anal. Online* **2006**, *22*, 209−210.
(27) Pluth, J. J.; Smith, J. V. Crystal structure of dehydrated potassium-exchanged zeolite A. Absence of supposed zero-coordinated potassium. refinement of silicon, aluminum-ordered superstructure. *J. Phys. Chem.* **1979**, *83*, 741−749.
(28) Newsam, J. M. Structures of dehydrated potassium zeolite L at 298 and 78 K containing sorbed perdeuteriobenzene. *J. Phys. Chem.* **1989**, *93*, 7689−7694.
(29) Simoncic, P.; Armbruster, T. Peculiarity and defect structure of the natural and synthetic zeolite mordenite: A single-crystal X-ray study. *Am. Mineral.* **2004**, *89*, 421−431.
(30) Chubynsky, M. V.; Thorpe, M. F. Self-organization and rigidity in network glasses. *Curr. Opin. Solid State Mater. Sci.* **2001**, *5*, 525−532.
(31) Sartbaeva, A.; Wells, S. A.; Treacy, M. M.; Thorpe, M. F. The flexibility window in zeolites. *Nat. Mater.* **2006**, *5*, 962−965.

https://doi.org/10.1021/acsomega.3c02882
ACS Omega 2023, 8, 32536−32543